Strong hyperfine-induced modulation of an optically driven hole spin in an InAs quantum dot

S. G. Carter,[1] Sophia E. Economou,[1] A. Greilich,[2,*] Edwin Barnes,[3] T. Sweeney,[4,*] A. S. Bracker,[1] and D. Gammon[1]

[1]*Naval Research Laboratory, Washington, D.C. 20375, USA*

[2]*University of Maryland contractor at the Naval Research Laboratory, Washington, D.C. 20375, USA*

[3]*Condensed Matter Theory Center, Department of Physics, University of Maryland, College Park, Maryland 20742-4111, USA*

[4]*National Research Council Research Associate at the Naval Research Laboratory, Washington, D.C. 20375, USA*

(Received 9 July 2013; revised manuscript received 8 February 2014; published 28 February 2014)

Compared to electrons, holes in InAs quantum dots have a significantly weaker hyperfine interaction that leads to less dephasing from nuclear spins. Thus many recent studies have suggested that nuclear spins are unimportant for hole-spin dynamics compared to electric-field fluctuations. We show that the hole hyperfine interaction can have a strong effect on hole-spin coherence measurements through a nuclear feedback effect. The nuclear polarization is generated through a unique process that is dependent on the anisotropy of the hole hyperfine interaction and the coherent precession of nuclear spins, giving rise to strong modulation at the nuclear precession frequency.

DOI: 10.1103/PhysRevB.89.075316 PACS number(s): 78.67.Hc, 42.50.Ex, 76.70.Hb, 78.47.jm

I. INTRODUCTION

The hyperfine interaction between electron spins and nuclear spins in solid-state materials has been of particular interest over the past decade, largely driven by a desire to take advantage of electron spins as quantum bits [1]. For electron spins in quantum dots (QDs), the hyperfine interaction with a bath of nuclear spins is the dominant source of dephasing as fluctuations in the nuclear polarization induce fluctuations in the electron-spin precession frequency through the Overhauser shift [2,3]. For holes, however, the contact hyperfine interaction, which dominates for electron spins, is suppressed due to the p orbital symmetry of the top of the valence band. The dipole-dipole hyperfine interaction is still present, but it is an order of magnitude weaker and is very anisotropic [4–9], leading to hopes of a highly coherent hole-spin qubit.

Recent experimental results in InAs QDs have yielded several disparate values for the heavy-hole inhomogeneous dephasing time T_2^*, ranging from 2 ns to values exceeding 100 ns [10–15], significantly longer than the 1–2 ns dephasing time for electron spins in these QDs [16]. The homogeneous dephasing time T_2 has been measured as 1 μs [13,17], with a spin relaxation time of 1 ms [18,19]. Experimental techniques and capabilities developed for electron spins in QDs, including ultrafast optical single-qubit and two-qubit gates in coupled QDs [20], have also been demonstrated for hole spins [12]. While the hole spin shows promise as a spin qubit [21–23], the influence of nuclear spins on hole-spin dynamics and the ability of holes to generate a nuclear polarization are still unclear. Because the hole hyperfine interaction is weaker compared to electrons, much recent work has suggested that nuclear spins are unimportant in hole-spin dynamics compared to the effects of fluctuating electric fields.

Here we demonstrate that nuclear spins can have a strong effect on optically controlled hole spins in QDs. We present Ramsey fringe and spin-echo measurements of a single heavy-hole spin in an InAs QD that show a strong amplitude modulation at the nuclear-spin precession frequency. The modulation frequency scales with the external magnetic field and matches twice the Larmor precession frequency of indium nuclear spins. Contrary to intuition, the effect is not due to a time-dependent Overhauser shift of the hole spin at the nuclear precession frequency since the hole hyperfine interaction is too weak. Instead, the hole spins generate a significant nuclear-spin polarization through a novel mechanism that depends on the phase of nuclear spins precessing in an external magnetic field and the anisotropy of the interaction. This nuclear polarization then indirectly affects the hole spin by shifting the optical transitions of the hole-spin system through the Overhauser shift of the *electron* in the positively charged trion, which is much greater than that of the hole. A theoretical model provides qualitative agreement with the experimental results. These results demonstrate that nuclear-spin effects can be quite important in hole-spin dynamics and that coherent precession of nuclear spins can strongly influence the polarization process.

II. EXPERIMENT

A. System

Our experiments are performed on a single pair of vertically stacked, coupled InAs QDs grown on a $p+$ GaAs substrate by molecular-beam epitaxy. The QDs are embedded in a p-type Schottky diode with a p-type beryllium-doped buffer layer grown on the substrate, followed by a 25 nm GaAs spacer barrier, two InAs QD layers of 2.8 and 3.2 nm thickness with a 6 nm tunnel barrier, and a 280 nm GaAs capping layer [see Fig. 1(b)]. (This is the same coupled QD system studied in Ref. [12]). A 5 nm layer of titanium and 120 nm of aluminum are evaporated onto the surface, forming a Schottky gate, with 1 μm apertures in the aluminum to isolate individual coupled QDs. The sample is held at a temperature of 6–7 K in a magneto-optical cryostat, with the magnetic field perpendicular to the growth direction [Fig. 1(a)]. Photoluminescence and optical transmission spectra of this coupled QD system have been presented in Ref. [12], in which the different charge

*Present address: Experimentelle Physik 2, Technische Universität Dortmund, D-44221 Dortmund, Germany.

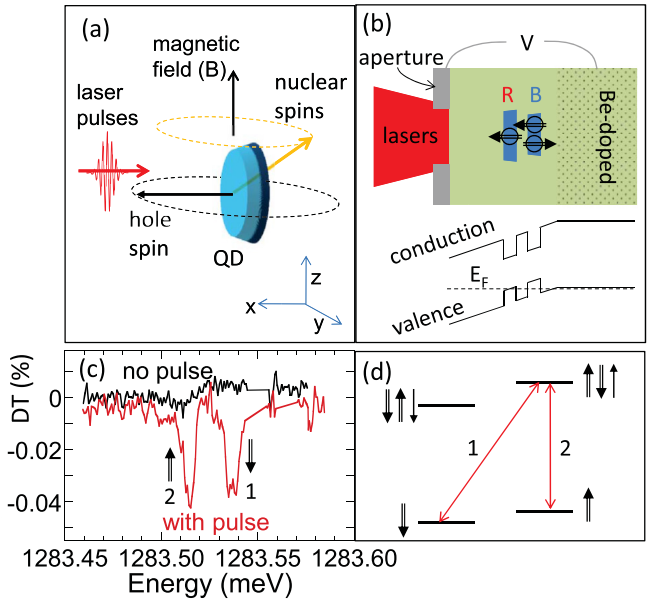

FIG. 1. (Color online) (a) Orientation of the InAs QD and the precessing hole and nuclear spins with respect to the optical axis and magnetic field. (b) Diagram of the QD molecule embedded within a Schottky diode, with the band diagram illustrated below. (c) Differential transmission of the QD at a magnetic field of 5 T, with and without a short pulse to defeat optical pumping. (d) Hole-trion level diagram in a Voigt magnetic field, with single (double) arrows representing electron (hole) spins.

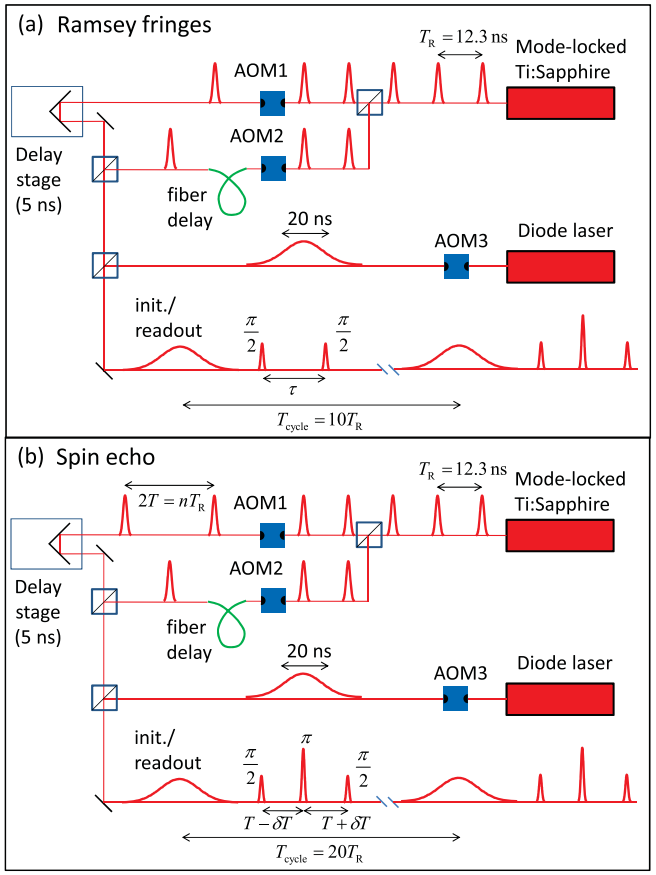

FIG. 2. (Color online) Experimental setup for generating the pulse sequences for (a) Ramsey fringes and (b) spin echoes.

configurations are observed as a function of the Schottky gate bias. All of the experiments reported in this work are at a bias of −0.236 V, where the bottom QD is charged with two holes and the top QD is charged with a single hole. With the two bottom QD holes in the singlet state and minimal coupling between QDs at this bias, the only spin degree of freedom is for the single heavy-hole spin in the top QD. We therefore consider the system as a single QD charged with a single hole. The presence of the bottom QD has the advantage that the optical linewidths (8 μeV) are significantly improved over our single QD samples, which we tentatively attribute to screening of charge fluctuations of nearby beryllium acceptors [24,25].

The hole spin is initialized, controlled, and measured using the optical transitions from the two hole-spin states to the two charged exciton (trion) states displayed in Fig. 1(d). We make use of the Lambda system formed by the two spin states of the hole and the upper trion state. The differential transmission (DT) spectrum of the upper two trion transitions is displayed in Fig. 1(c). In this technique (see Ref. [26]), the sample bias is modulated with a square wave of amplitude 400 mV and frequency 10 kHz, and the transmitted laser signal is sent to a lock-in amplifier. The modulation amplitude is large enough to bring the QD system out of the triply charged state, modulating the trion absorption. When the laser is tuned over the transitions, optical pumping occurs and the absorption goes to zero [black curve in Fig. 1(c)] [19,27,28]. In the presence of a short, spin rotation pulse, optical pumping is defeated and the two absorption lines are visible (red curve). This DT spectrum provides a rough calibration for spin polarization in the Ramsey fringe and spin-echo experiments. Assuming no optical pumping and equal spin populations under these conditions, −0.08% DT on transition 1 should correspond to fully spin down, and 0% to fully spin up [29].

B. Ramsey fringe measurement

Figure 2 displays the experimental setup used to generate the pulse sequences for Ramsey fringe and spin-echo measurements. In both cases, two acousto-optic modulators (AOMs) are used to pick pulses from the Spectra-Physics Tsunami Ti:sapphire laser operating at 81 MHz. These AOMs are used to extend the experimental cycle time T_{cycle} beyond the laser repetition period $T_R = 12.3$ ns. These short (13 ps, 150 μeV bandwidth), circularly polarized pulses are used to optically rotate the spin state about the optical axis. The pulses are detuned below the lowest energy transition by 200–300 μeV to rotate the hole-spin state through a virtual process [30–36]. A third AOM is used to modulate an external cavity diode laser tuned to transition 1, producing 20 ns narrowband pulses that simultaneously optically pump the QD into the hole spin up state $|\Uparrow\rangle$ and measure the spin down $|\Downarrow\rangle$ population using DT. The short pulses and narrowband pulses have opposite circular polarizations, such that the short pulses are rejected by a polarizer before hitting the detector.

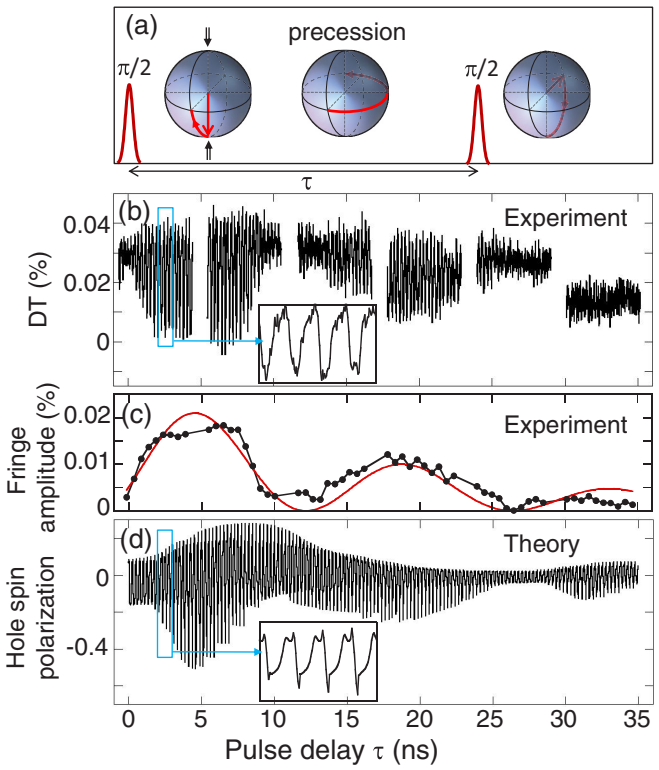

FIG. 3. (Color online) (a) Ramsey fringe pulses with illustration of the evolution of the hole spin on the Bloch sphere. (b) Ramsey fringes at 4 T. (c) Fringe amplitude vs delay obtained from the data in (b), with a decaying cosine fit. (d) Theoretically calculated Ramsey fringes at 4 T multiplied by an exponential decay with a 20 ns decay time. The hole hyperfine interaction is nearly Ising along the growth direction ($A_x^h = 1.05$ neV), with an anisotropy of 90%. The insets in (b) and (d) magnify a 1 ns delay window for experiment and theory to display the fringe shape.

Hole-spin dynamics are first measured using Ramsey interference fringes, in which the delay between two optical spin rotation pulses is varied while measuring the resulting spin population [30]. As displayed in Fig. 2(a), 30–50 ns after the initialization pulse, AOM1 and AOM2 select two $\pi/2$ rotation pulses, which can be delayed relative to another by a multiple of T_R using pulse picking, by $\sim T_R/2$ to one another using a fiber delay, and by a variable delay of 0–5 ns using a motorized delay stage. In this way, the delay τ can be varied nearly continuously over time scales much longer than T_R. Here the pulse sequence period T_{cycle} is 123 ns. As shown in the Bloch spheres of Fig. 3(a), the first $\pi/2$ pulse rotates the hole spin to the equator, where it precesses about the applied magnetic field. The second $\pi/2$ pulse brings the hole spin closer to $|\Uparrow\rangle$ or $|\Downarrow\rangle$ on the Bloch sphere, depending on the spin phase at the second pulse. In the absence of nuclear feedback, the spin down $|\Downarrow\rangle$ population, measured with DT, should give exponentially decaying sinusoidal oscillations at the Larmor precession frequency of the hole. Figure 3(b) displays Ramsey fringes at a magnetic field of 4 T, showing hole-spin precession at 4 GHz (g factor of 0.071) and a slow amplitude modulation at $\sim$70 MHz. The inset of Fig. 3(b) plots these same Ramsey fringes over a small delay range from 2–3 ns to better display hole-spin fringes. The fringes have a sawtooth shape that we attribute to a nuclear polarization that depends on the pulse delay. The nuclear polarization shifts the optical transitions relative to the laser, primarily due to the Overhauser shift of the unpaired electron spin in the trion state, which is significantly larger than that of the hole-spin states. These shifts weaken the initialization and measurement process and distort the fringes. This delay-dependent nuclear polarization effect is similar to that observed for electron spins [37] and will be used to explain the slow modulation.

A striking feature of our data is the strong amplitude modulation of the fringes. Figure 3(c) plots the fringe amplitude vs delay, obtained by fitting every two fringes to a cosine, showing a strong modulation at 70 MHz with a decay time T_2^* of 19 ns. We attribute the modulation to a significant nuclear polarization that is generated when the delay τ matches half-integer multiples of the nuclear precession period (at 0, 12, and 26 ns), as will be explained below. With several different nuclear species present (^{69}Ga, ^{71}Ga, ^{75}As, ^{113}In, and ^{115}In), modulation could occur at several frequencies, but ^{115}In is expected to dominate due to its large nuclear spin of 9/2 and high abundance. The expected ^{115}In precession frequency is 37.5 MHz at 4 T [38], which is roughly half the observed modulation frequency. In Fig. 3(d), a theoretical calculation of the Ramsey fringes, which takes into account the interaction with nuclear spins, qualitatively reproduces this modulation, as will be discussed below. The modulation is also observed at a magnetic field of 6 T with a frequency of 112 MHz, roughly scaling with the magnetic field. At a bias of -0.245 V, where coupling to the bottom QD should be even weaker, the modulation was measured with no discernible change in frequency, indicating that the effect is not sensitive to the tunnel coupling. Ramsey fringe measurements in another pair of coupled QDs also showed modulation at the same frequency but with a weaker amplitude.

C. Spin-echo measurements

Spin-echo measurements were performed to further characterize this behavior and eliminate the effects of inhomogeneous dephasing. As displayed in Fig. 2(b), a higher intensity pulse yielding a π rotation of the hole spin is inserted between the two $\pi/2$ pulses, with nearly equal delays of $T - \delta T$ and $T + \delta T$ between adjacent pulses. We expect inhomogeneous dephasing of this system due to fluctuations in the nuclear-spin polarization or in the charge environment. If these fluctuations are slow compared to T, the π pulse rephases the system, giving a spin echo. The echo amplitude is measured by essentially the same technique used in [16], in which the two $\pi/2$ pulses are delayed with respect to the π pulse. The two $\pi/2$ pulses are selected by AOM1, with a delay set to $2T = nT_R$, where n is an integer. The π pulse is selected by AOM2 and set to the midpoint of the two $\pi/2$ pulses (using the $T_R/2$ fiber delay for odd values of n). As shown in Fig. 4(a), a small delay offset δT shifts the π pulse away from the midpoint to scan the third pulse (at $2T$) relative to the echo, which should occur at $2(T - \delta T)$. Thus, the fringe frequency is doubled due to the $2\delta T$ echo delay. Typically, the spin echo will monotonically decay as a function of T, according to the homogeneous dephasing time T_2. Figure 4(b) plots the spin-echo signal at 4 T as a function of δT for a series of

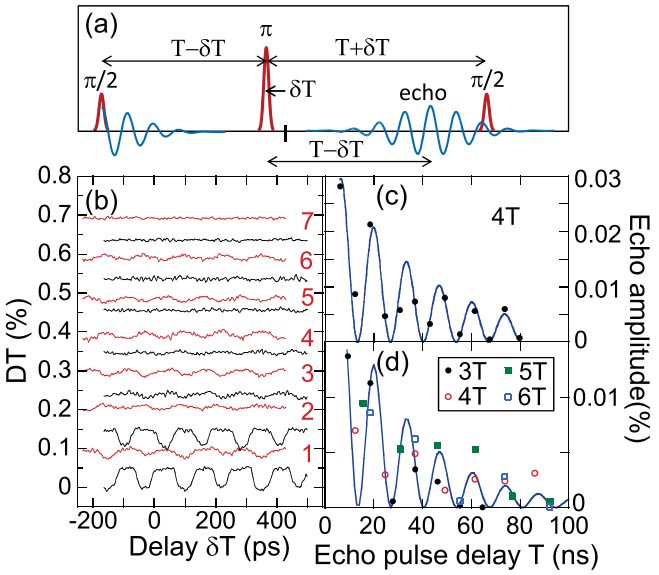

FIG. 4. (Color online) (a) Pulse timing diagram of the spin-echo measurement showing the delay between the spin echo and the second $\pi/2$ pulse. Blue oscillations represent the precessing spin polarization. (b) Ramsey fringe echo signal at B = 4 T as a function of δT for a series of values of T, which are labeled in units of $T_R = 12.3$ ns for red/gray curves. Black curves are half-integer steps of T_R. $T_{\text{cycle}} =$ 246 ns (c) Echo amplitude vs T, obtained from fitting the data in (b). (d) Echo amplitude vs T for several magnetic fields, in which the T is scaled by the magnetic field according to $T \rightarrow (B/4)T$. Fits of the data in (c) and (d) to a decaying cosine are shown as solid lines.

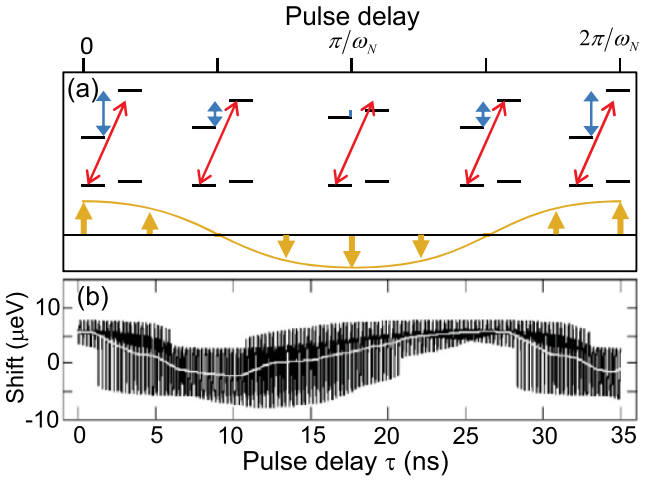

FIG. 5. (Color online) (a) Illustration of how the nuclear polarization (yellow arrows) modulates initialization and measurement of the hole spin through the Overhauser shift of the trion. The level diagrams display the hole (lower) and trion (upper) energy levels and the initialization/readout laser for different nuclear polarizations. (b) Theoretically calculated Overhauser shift of the trion for the same parameters as in Fig. 3(d), with the white line smoothing over the fast oscillations.

echo pulse delays T. The amplitude and phase of the echo are significantly modulated as a function of T. The amplitude of the echo is plotted as a function of T in Fig. 4(c), with a fit to a decaying sinusoidal function, $A\exp(-2T/T_2)[1-\cos(\Omega T)]$, which gives $T_2 = 74$ ns and $\Omega = 73.6$ MHz. This modulation has nearly the same frequency and presumably the same origin as the modulation in the Ramsey fringes. Spin-echo measurements were also performed for a series of magnetic fields from 3–6 T to test how well the modulation scales with magnetic field. The amplitudes vs T for all fields are plotted in Fig. 4(d), with the delays scaled to T for each data set. [The delays at magnetic field B were scaled $T \longrightarrow (B/4)T$.] Most of the points fall on the decaying oscillation rather well with fit parameters of $T_2 = 58$ ns and $\Omega = 74.6$ MHz, indicating that the modulation scales with the magnetic field as expected for a modulation mechanism that depends on nuclear-spin precession.

III. THEORY

At first glance, the Ramsey fringe and echo modulation observed here might naively be attributed to a precessing nuclear-spin polarization that periodically modifies the hole-spin precession frequency, which is commonly observed for electron spins in solid-state systems [39]. For this effect to occur, a significant hyperfine interaction is necessary as well as nuclear precession about a different quantization axis than that of the resident electrons or holes. This type of spin-echo modulation has been observed for electrons in electrically defined QDs in GaAs at low magnetic fields, disappearing above 0.2 T [40], and theoretically predicted for holes in QDs at low magnetic fields [41]. These effects become negligible at the high magnetic fields used here, where the hole- and nuclear-spin quantization axes are fixed by the strong field and the hole hyperfine interaction is weak relative to the Zeeman terms.

Instead, we attribute the modulation observed here to the generation of a significant nuclear polarization when the optical pulse delay τ matches the precession of indium nuclear spins. As illustrated in Fig. 5(a), the nuclear polarization shifts the optical transition out of resonance with the initialization/measurement laser due to the Overhauser shift of the trion spin states. This periodically reduces the generated hole-spin polarization and thus the amplitude of the fringes. For a nuclear polarization oscillating positive and negative each period, the amplitude is reduced twice per period. (Note that the nuclear polarization is not changing on a nanosecond time scale. Instead, a different polarization builds up at each pulse delay, which is changed about once per second.)

A. Toy model

The origin of the nuclear polarization can be understood conceptually from a physical picture with two spins, i.e., one hole and one nuclear spin, with a Hamiltonian $H = \omega_h S_z + \omega_N I_z + A_x^h S_x I_x$. The hole- and nuclear-spin splittings are ω_h and ω_N with spin operators S and I, and the hyperfine interaction A^h is approximated as Ising-like. The effects of optical pulses are not included in this picture, but they act to collapse the system after the evolution time. The evolution can be described by two pseudospins, one corresponding to the two states in which the hole and nuclear spins are parallel and one corresponding to the two states in which they are antiparallel.

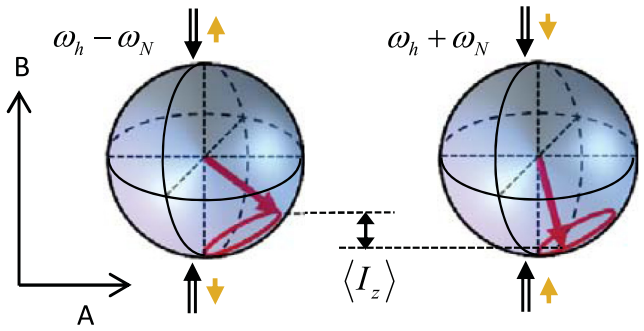

FIG. 6. (Color online) The two Bloch spheres representing the interacting hole-nuclear spin system that gives rise to a nuclear polarization, with double arrows representing the hole spin and short single arrows representing a nuclear spin. The Ising-like hyperfine interaction is perpendicular to the quantization axis along the magnetic field. The equal statistical mixture of both pseudospins pointing along the south poles represents a fully polarized hole and an unpolarized nuclear spin.

The Bloch spheres for these pseudospins are shown in Fig. 6. The two Bloch vectors evolve independently in the absence of optical pulses and with precession frequencies $\omega_h \pm \omega_N$. The hyperfine interaction causes the Bloch vectors to precess about an axis tilted with respect to the North-South axis. If we start in $|\Uparrow \downarrow\rangle$, the pseudospin precesses about the tilted axis, giving a small time-dependent probability of $|\Downarrow \uparrow\rangle$. Measurement of the hole spin projects the system into $|\Uparrow \downarrow\rangle$ or $|\Downarrow \uparrow\rangle$, giving a small probability w_+ of a hole-nuclear flip-flop that oscillates at $\omega_h - \omega_N$. The same occurs starting in $|\Uparrow \uparrow\rangle$, with a flip-flop rate w_- that oscillates at $\omega_h + \omega_N$. The difference in these spin flip rates oscillates at ω_N, which gives rise to a nuclear polarization that depends on the hole-nuclear evolution time.

B. Full model

While the main qualitative feature of the data, i.e., the modulation at the indium precession frequency, can be understood via this physical picture, a more sophisticated approach along the lines of Ref. [42] is needed to model the full dynamics of the hole as modified by the net nuclear bath. These dynamics are generated by the Hamiltonian

$$H = H_0 + H_p + H_{\rm rad} + H_{hf}, \tag{1}$$

where

$$H_0 = \omega_h S_z + \sum_{j=\uparrow,\downarrow} \epsilon_{T_j} |T_j\rangle\langle T_j| + \omega_N \sum_i I_z^i,$$

$$H_p = \Omega_1(t)|\bar{z}\rangle\langle T_\uparrow| + [\Omega_{\pi/2}(t) + \Omega_{\pi/2}(t+\tau)]|x\rangle\langle T_\uparrow| + \text{H.c.},$$

$$H_{\rm rad} = \sum_k g_k(|\bar{z}\rangle\langle T_\uparrow| + |z\rangle\langle T_\uparrow|)a_k^\dagger e^{i\omega_k t} + \text{H.c.},$$

$$H_{hf} = \sum_i \left(A_x^h S_x I_x^i + A_\perp^h S_y I_y^i + A_\perp^h S_z I_z^i + A^e \mathbf{J}\cdot\mathbf{I}^i\right),$$

where S_j, I_j, J_j are the hole, nuclear, and trion spin operators along the j axis, respectively (the heavy-hole states are approximated as a pseudospin). The magnetic field defines the quantization axis z. $\Omega_1(t)$ denotes the long pulse, $\Omega_{\pi/2}(t)$ denotes the $\pi/2$ δ pulses, $|z\rangle(|\bar{z}\rangle)$ is the hole spin up (down) state along the B-field direction, $|x\rangle$ is the hole spin up state along the optical axis x, $|T_\uparrow\rangle$ ($|T_\downarrow\rangle$) is the excited trion state with spin up (down) along the z axis, g is the coupling to the radiation bath, and $a^\dagger$ is the bath photon creation operator. The different A's (A_x^h and $A_\perp^h$) indicate that the hole-nuclear hyperfine interaction is anisotropic, with the optical/growth axis component being stronger, i.e., $A_x^h \gg A_\perp^h$. A^e denotes the hyperfine interaction between the trion (which carries the spin of the electron, as the two holes form a spin singlet) and the nuclear spin. In writing the above expressions, we have made the approximation that the hyperfine couplings are the same for every nucleus ("box model"). We also approximate the measurement/initialization pulse to be a square pulse, as shown in Fig. 7.

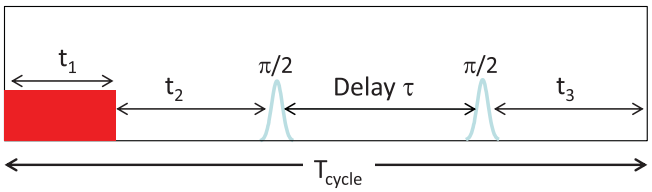

FIG. 7. (Color online) Pulse sequence used in the theory.

The main idea of the theory is that the laser-generated hole polarization is transferred to the nuclear spins via the joint hole-nuclear evolution under the hyperfine interaction and the B field. Subsequent hole-spin measurement disentangles the joint quantum state, collapsing it to a state with finite nuclear polarization. At each delay τ, a steady-state nuclear polarization P is thus generated over many pulse repetition cycles. The nuclear polarization relies on optical excitation of the trion, so it depends on the detuning Δ of the narrowband laser from the QD transition. But this detuning itself depends on the nuclear polarization through the Overhauser shift of the unpaired electron in the trion state, giving rise to a feedback effect. Thus, Δ and P must be found self-consistently, i.e., they must satisfy the equation

$$\Delta(\tau) = A^e P(\Delta, \tau). \tag{2}$$

Once we obtain Δ, we can find the hole-spin state as a function of the delay.

In order to find the detuning $\Delta(\tau)$, we need to first determine the dependence of the nuclear polarization on an arbitrary detuning δ, $P(\delta,\tau)$. We proceed to find this by making use of the independent nuclear-spin approximation. In particular, we first find for an arbitrary detuning the joint evolution of one nuclear spin (with two states, up and down) coupled to the hole spin, and from this extract the steady state of each spin. The steady state is the relevant quantity because the experimental signal is accumulated over a large number of cycles. The first goal is to compute the two-spin evolution over one pulse train period (Fig. 7). This is done by breaking up this evolution into two parts: the unitary part, which corresponds to free evolution (no optical excitation) and the two $\pi/2$ pulses, and the nonunitary part, which consists of the longer measuring/initializing pulse. Once we have the evolution after one pulse cycle, we can derive from this the steady state

after many such cycles. The total nuclear polarization is obtained from $P = N\langle I_z\rangle$, where $\langle I_z\rangle$ is the z component of the nuclear-spin steady state and N is the number of In nuclei. This is essentially a mean-field approach. A detailed discussion of this procedure is given in the Appendix.

Before we proceed to compare our theoretical results with the experimental data, we would first like to point out some important differences between the present model and the theory developed in Refs. [42,43]. These differences primarily stem from the fact that here we have a longer pulse and not just δ pulses. The Markovian approximation of [42,43] is not as well justified here due to the fact that the effective detuning (coming from the Overhauser shift of the positively charged trion) can become large and weaken the response of the system to the longer, narrowband pulses. In other words, the effect of the pulses is not consistently disruptive so as to justify the Markovian approximation (see Fig. 4 of Ref. [42]). For this reason, in the present work we have developed a non-Markovian model by solving simultaneously for the hole- and nuclear-spin evolutions.

There is a conceptual similarity between the feedback mechanism in our theory and that of Ref. [44], where the ground state was an electron spin and the spin state of the trion was determined by the unpaired hole. Compared to the present case, that scenario can be thought of as the electron and hole switching roles; in both cases, however, the feedback process is caused by the combination of the nuclear-spin interaction with the anisotropic hole (that gives rise to nuclear spin flips) and the Overhauser term of the *electron* spin.

C. Comparison to experiment

In Fig. 3(d), we plot the spin component of the hole along the B field as a function of the delay, simulating the Ramsey fringes. Figure 5(b) displays the Overhauser shift of the trion, showing the fast oscillations that give the sawtooth shape and the slow oscillations that give the modulation at the nuclear frequency. We can thus reproduce the salient features of the experiment. The theory also helps explain why this effect has not been previously observed for electrons or holes. The theory shows that an isotropic hyperfine interaction, which is the case for electrons, gives essentially no fringe modulation. A larger hole g factor also reduces the modulation. Since these parameters are quite dependent on the geometry of the QD, this may explain why a similar experiment with different QDs by another group did not observe hole-spin echo modulation [13]. There, the g factor was 0.27, about four times larger than for our holes, and the trion linewidths were 3.5 times ours, making the experiment less sensitive to Overhauser shifts. This theory also produces modulation of the echo signal when a π pulse is added with the same physical explanation. However, the change in phase with T observed in Fig. 4(b) is not produced by the theory and is not yet understood.

IV. CONCLUSIONS

The results presented here demonstrate that while the hole hyperfine interaction is weaker than for electrons, resulting in a longer T_2^*, the hole hyperfine interaction can still generate a nuclear polarization that has a strong effect on hole-spin measurement and initialization. The generation of the nuclear polarization is a result of the anisotropic hyperfine interaction that is stronger along the growth direction. The strength of the nuclear polarization is also sensitive to the phase of the nuclear-spin precession with respect to the optical pulses [45], another indication of the rich physics of this system. Interestingly, our theoretical model indicates that the direct effect of this nuclear polarization on the hole spin is minimal, and that the dominant effect on the hole is from the Overhauser shift of the electron spin in the trion state, which shifts the optical transition frequency out of resonance with the initialization and measurement laser and thus reduces the hole-spin amplitude. This suggests that the T_2^* measured here is not limited by nuclear-spin fluctuations but instead by charge fluctuations, as discussed previously [12]. However, the measured echo decay time is shorter than values obtained in a similar system [13], which may be due to inhomogeneity of the indium nuclear precession frequency and/or contributions from gallium and arsenic nuclear spins that wash out the echo. The improved understanding of this rich physical system developed here should significantly help in improving hole spins as qubits and could also be used to optically control the nuclear-spin polarization [37,46,47].

ACKNOWLEDGMENTS

This work was supported by a Multi-University Research Initiative (U.S. Army Research Office, Grant No. W911NF0910406), the NSA/LPS, and the U.S. Office of Naval Research.

APPENDIX: DETAILED THEORY

Here we provide a detailed treatment of the theory outlined in the main text. We begin by computing the unitary part of the evolution. We can rewrite the Hamiltonian to only include one nuclear spin by simply dropping the sums (and the i indices) in H_0 and H_{hf}. We define the two-spin Zeeman and hyperfine Hamiltonian, which describes the free evolution of the system (without optical excitation), as

$$H_{hn} = \omega_h S_z + \omega_N I_z + A_x^h S_x I_x + A_\perp^h S_y I_y + A_\perp^h S_z I_z.$$

The evolution operator for the unitary part of the evolution is then

$$U_{hn} = e^{-iH_{hn}t_3} R_x(\pi/2) e^{-iH_{hn}\tau} R_x(\pi/2) e^{-iH_{hn}t_2}. \tag{A1}$$

Since we will eventually combine this with the nonunitary part of the evolution, it is necessary to go to the spin-vector representation of the state (see Ref. [42]): $\mathcal{S}_i = 4\mathrm{Tr}(\rho G_i)$, where ρ is the 4×4 density matrix of the two spins, and the generators G_i are tensor products of spin operators (including the identity) $G_{4k+\ell} = S_k \otimes I_\ell$, where k,ℓ run from 0 to 3. With our conventions, $\mathcal{S}_0 = 1$. We may construct an evolution operator which acts directly on the spin vector as follows:

$$Y_{U,ij} = 4\mathrm{Tr}[G_i U_{hn} G_j U_{hn}^\dagger], \tag{A2}$$

so that $\mathcal{S}(T_{\mathrm{cycle}}) = Y_U \mathcal{S}(t_1)$.

We next consider the nonunitary part of the evolution. Although we have reduced the problem to a two-spin system, it is still highly nontrivial because of the coupling to the

photonic bath described by H_r. Our general approach will be to introduce operators that describe the combined action of the long pulse and the photonic bath that allow us to eliminate the trion state while keeping its contributions to the spin dynamics. This is essentially the formalism we developed earlier for pulsed excitation [42]. Here we will adapt it to take into account the extra effects originating from the long pulse excitation.

The Hamiltonian describing the free (nondriven) evolution of the system is

$$H_{lf} = \begin{pmatrix} H_{gs} & 0 \\ 0 & H_{es} \end{pmatrix}, \tag{A3}$$

$$H_{gs} = \begin{pmatrix} \frac{\omega_h}{2} + \frac{\omega_N}{2} + \frac{A^h_\perp}{4} & 0 & 0 & \frac{A^h_x - A^h_\perp}{4} \\ 0 & \frac{\omega_h}{2} - \frac{\omega_N}{2} - \frac{A^h_\perp}{4} & \frac{A^h_x + A^h_\perp}{4} & 0 \\ 0 & \frac{A^h_x + A^h_\perp}{4} & -\frac{\omega_h}{2} + \frac{\omega_N}{2} - \frac{A^h_\perp}{4} & 0 \\ \frac{A^h_x - A^h_\perp}{4} & 0 & 0 & -\frac{\omega_h}{2} - \frac{\omega_N}{2} + \frac{A^h_\perp}{4} \end{pmatrix},$$

$$H_{es} = \begin{pmatrix} \epsilon_{T_\uparrow} + \delta + \frac{\omega_N}{2} + \frac{A^e}{4} & 0 & 0 & 0 \\ 0 & \epsilon_{T_\uparrow} + \delta - \frac{\omega_N}{2} - \frac{A^e}{4} & \frac{A^e}{2} & 0 \\ 0 & \frac{A^e}{2} & \epsilon_{T_\downarrow} - \delta + \frac{\omega_N}{2} - \frac{A^e}{4} & 0 \\ 0 & 0 & 0 & \epsilon_{T_\downarrow} - \delta - \frac{\omega_N}{2} + \frac{A^e}{4} \end{pmatrix}, \tag{A4}$$

where H_{gs} is in the basis $|zn_\uparrow\rangle$, $|zn_\downarrow\rangle$, $|\bar{z}n_\uparrow\rangle$, $|\bar{z}n_\downarrow\rangle$, and H_{es} is in the basis $|T_\uparrow n_\uparrow\rangle$, $|T_\uparrow n_\downarrow\rangle$, $|T_\downarrow n_\uparrow\rangle$, $|T_\downarrow n_\downarrow\rangle$, with $\epsilon_{T_\uparrow} = \omega - \omega_h/2$, $\epsilon_{T_\downarrow} = \omega - \omega_h/2 - \omega_e$. Here, ω is the frequency of the long pulse, ω_e is the Zeeman frequency of the trion due to the unpaired electron, and $|n_{\uparrow,\downarrow}\rangle$ are the spin states of the nucleus. In Eq. (A4), δ is the detuning of the long pulse from the driven transition. This detuning is one of the key features of the physics in this problem: It is proportional to the Overhauser shift of the unpaired electron in the trion state, as shown in Fig. 5(a) of the main text. The detuning Δ will be determined self-consistently by computing the resulting nuclear polarization and equating it to $\Delta/(A^e N)$. Note that we use δ as a variable and reserve the symbol Δ for the self-consistently determined detuning.

We now describe how to find the dynamical map describing the nuclear-hole evolution due to the long pulse and spontaneous emission. The Hamiltonian of the system during the time interval t_1 is

$$H_1 = H_{lf} + \Omega_1(t)|\bar{z}\rangle\langle T_\uparrow| + \Omega_1^*(t)|T_\uparrow\rangle\langle\bar{z}|, \tag{A5}$$

with $\Omega_1(t) = \Omega_0 e^{i\omega t}$. We transform H_1 to a rotating frame using the operator $\mathcal{T} = \left(\begin{smallmatrix} U_{gs} & 0 \\ 0 & U_T \end{smallmatrix}\right)$, where $U_{gs} = e^{-iH_{gs}t}$ and

$$U_T = \begin{pmatrix} e^{i(\omega-\omega_h/2+\omega_N/2)t} & 0 & 0 & 0 \\ 0 & e^{i(\omega-\omega_h/2-\omega_N/2)t} & 0 & 0 \\ 0 & 0 & e^{i(\omega-\omega_h/2-\omega_N/2)t} & 0 \\ 0 & 0 & 0 & 1 \end{pmatrix}. \tag{A6}$$

This transformation allows us to eliminate the time dependence and obtain the following effective Hamiltonian:

$$H_{\text{eff}} = \begin{pmatrix} 0 & 0 & 0 & 0 & 0 & 0 \\ 0 & 0 & 0 & 0 & 0 & 0 \\ 0 & 0 & 0 & 0 & \Omega_0 & 0 \\ 0 & 0 & 0 & 0 & 0 & \Omega_0 \\ 0 & 0 & \Omega_0 & 0 & \frac{A^e}{4} + \delta & 0 \\ 0 & 0 & 0 & \Omega_0 & 0 & -\frac{A^e}{4} + \delta \end{pmatrix}. \tag{A7}$$

The spontaneous emission is described by Lindblad operators:

$$\begin{aligned} \mathcal{L}_1 &= \gamma\mathcal{T}(|zn_\uparrow\rangle\langle T_\uparrow n_\uparrow| + |\bar{z}n_\uparrow\rangle\langle T_\uparrow n_\uparrow|)\mathcal{T}^\dagger, \\ \mathcal{L}_2 &= \gamma\mathcal{T}(|zn_\downarrow\rangle\langle T_\uparrow n_\downarrow| + |\bar{z}n_\downarrow\rangle\langle T_\uparrow n_\downarrow|)\mathcal{T}^\dagger, \end{aligned} \tag{A8}$$

where γ is the spontaneous-emission rate. In Eqs. (A7) and (A8), we have neglected the pulse- and spontaneous-emission-induced hyperfine flip-flops for both the hole and trion. This approximation is justified because $A^e\Omega_0/\omega_e^2 \ll 1$, $A^e\gamma/\omega_e^2 \ll 1$, $A^h_x\Omega_0/\omega_h^2 \ll 1$, and $A^h_x\gamma/\omega_h^2 \ll 1$. With this approximation, the state $|T_\downarrow\rangle$ decouples from the dynamics, and we henceforth ignore it. This approximation then allows us to treat the resulting six-level system as two independent three-level systems.

We solve each of these three-level systems for a range of detunings, constructing the dynamical map $Y_1(\delta)$. This is a 16-dimensional (16D) matrix (see Refs. [42,43]) which maps an arbitrary initial 16D hole-nuclear spin vector at the start of the long pulse to a final 16D spin vector at $t = t_1$. Combining this with the unitary part, Y_U, we can construct the dynamical map for a full period:

$$Y_{\text{cycle}}(\delta) = Y_{\text{decoh}} Y_U Y_{gs} Y_1(\delta), \tag{A9}$$

where $Y_{gs,ij} = 4\text{Tr}[G_i U_{gs} G_j U_{gs}^\dagger]$ has been included to transform the nonunitary part of the evolution back to the laboratory

frame, and where $Y_{\rm decoh}$ describes a phenomenological decay and dephasing process for the hole spin. This is constructed by first defining a pair of Kraus operators:

$$K_1 = \begin{pmatrix} 1 & 0 \\ 0 & e^{-T_{\rm cycle}/(2T_1)} \end{pmatrix}, \quad K_2 = \begin{pmatrix} 0 & \sqrt{1-e^{T_{\rm cycle}/T_1}} \\ 0 & 0 \end{pmatrix}. \tag{A10}$$

We then have

$$Y_{decoh,ij} = 4\sum_{\ell} \mathrm{Tr}[G_i(K_\ell \otimes \mathbb{1}_2)G_j(K_\ell \otimes \mathbb{1}_2)], \tag{A11}$$

where $\mathbb{1}_n$ denotes the $n \times n$ identity matrix.

Finally, for each value of the delay τ, we compute the hole-nuclear steady state $\mathcal{S}(\delta,\tau)$ numerically as a function of δ by computing the null eigenvector of $\mathbb{1}_{16} - Y_{\rm tot}(\delta)$ [42,43].

We then obtain the steady-state value of the detuning due to a large number of nuclear spins self-consistently by solving the equation

$$\Delta = A^e N \mathcal{S}_4(\Delta,\tau), \tag{A12}$$

where N is the number of nuclear spins, and $\mathcal{S}_4 = \langle I_z \rangle$ is the z component of the nuclear spin. For every τ, this fixes the detuning [48], and the hole-spin steady state and nuclear polarization can then be read off from $\mathcal{S}(\Delta,\tau)$. To produce Fig. 3(d), this procedure was followed using the following parameter values: $t_1 = 25.7$ ns, $t_2 = 50$ ns, $T_{\rm cycle} = 250.7$ ns, $B = 4$ T, $\Omega_0 = 0.88\ \mathrm{GHz}/(2\pi)$, $\gamma = 0.5$ GHz, $\omega_h = 8\pi\ \mathrm{GHz}/(2\pi)$, $\omega_N = 0.23\ \mathrm{GHz}/(2\pi)$, $A^e = 0.016\ \mathrm{GHz}/(2\pi)$, $A^h_x = A^e/10$, $A^h_\perp = A^h_x/10$, $N = 10\,000$, $T_1 = 2.3T_{\rm cycle}$, and $T_2^* = 20$ ns. Here, T_2^* is a phenomenological dephasing rate included in an overall factor, $e^{-\tau/T_2^*}$, multiplying the hole-spin steady state.

[1] B. Urbaszek, X. Marie, T. Amand, O. Krebs, P. Voisin, P. Maletinsky, A. Högele, and A. Imamoglu, Rev. Mod. Phys. **85**, 79 (2013).

[2] A. V. Khaetskii, D. Loss, and L. Glazman, Phys. Rev. Lett. **88**, 186802 (2002).

[3] I. A. Merkulov, A. L. Efros, and M. Rosen, Phys. Rev. B **65**, 205309 (2002).

[4] J. Fischer, W. A. Coish, D. V. Bulaev, and D. Loss, Phys. Rev. B **78**, 155329 (2008).

[5] B. Eble, C. Testelin, P. Desfonds, F. Bernardot, A. Balocchi, T. Amand, A. Miard, A. Lemaitre, X. Marie, and M. Chamarro, Phys. Rev. Lett. **102**, 146601 (2009).

[6] P. Fallahi, S. T. Yilmaz, and A. Imamoglu, Phys. Rev. Lett. **105**, 257402 (2010).

[7] J. Fischer and D. Loss, Phys. Rev. Lett. **105**, 266603 (2010).

[8] E. A. Chekhovich, A. B. Krysa, M. S. Skolnick, and A. I. Tartakovskii, Phys. Rev. Lett. **106**, 027402 (2011).

[9] E. A. Chekhovich, M. Glazov, A. Krysa, M. Hopkinson, P. Senellart, A. Lemaître, M. S. Skolnick, and A. I. Tartakovskii, Nat. Phys. **9**, 74 (2012).

[10] D. Brunner, B. D. Gerardot, P. A. Dalgarno, G. Wüst, K. Karrai, N. G. Stoltz, P. M. Petroff, and R. J. Warburton, Science **325**, 70 (2009).

[11] S. A. Crooker, J. Brandt, C. Sandfort, A. Greilich, D. R. Yakovlev, D. Reuter, A. D. Wieck, and M. Bayer, Phys. Rev. Lett. **104**, 036601 (2010).

[12] A. Greilich, S. G. Carter, D. Kim, A. S. Bracker, and D. Gammon, Nat. Photon. **5**, 702 (2011).

[13] K. D. Greve, P. L. McMahon, D. Press, T. D. Ladd, D. Bisping, C. Schneider, M. Kamp, L. Worschech, S. Höfling, A. Forchel *et al.*, Nat. Phys. **7**, 872 (2011).

[14] T. M. Godden, J. H. Quilter, A. J. Ramsay, Y. Wu, P. Brereton, S. J. Boyle, I. J. Luxmoore, J. Puebla-Nunez, A. M. Fox, and M. S. Skolnick, Phys. Rev. Lett. **108**, 017402 (2012).

[15] J. Houel, J. H. Prechtel, D. Brunner, C. E. Kuklewicz, B. D. Gerardot, N. G. Stoltz, P. M. Petroff, and R. J. Warburton, arXiv:1307.2000.

[16] D. Press, K. De Greve, P. L. McMahon, T. D. Ladd, B. Friess, C. Schneider, M. Kamp, S. Höfling, A. Forchel, and Y. Yamamoto, Nat. Photon. **4**, 367 (2010).

[17] S. Varwig, A. Schwan, D. Barmscheid, C. Müller, A. Greilich, I. A. Yugova, D. R. Yakovlev, D. Reuter, A. D. Wieck, and M. Bayer, Phys. Rev. B **86**, 075321 (2012).

[18] D. Heiss, S. Schaeck, H. Huebl, M. Bichler, G. Abstreiter, J. J. Finley, D. V. Bulaev, and D. Loss, Phys. Rev. B **76**, 241306 (2007).

[19] B. D. Gerardot, D. Brunner, P. Dalgarno, P. Ohberg, S. Seidl, M. Kroner, K. Karrai, N. G. Stoltz, P. Petroff, J. Houel *et al.*, Nature (London) **451**, 441 (2008).

[20] D. Kim, S. G. Carter, A. Greilich, A. S. Bracker, and D. Gammon, Nat. Phys. **7**, 223 (2011).

[21] S. E. Economou, J. I. Climente, A. Badolato, A. S. Bracker, D. Gammon, and M. F. Doty, Phys. Rev. B **86**, 085319 (2012).

[22] J. C. Budich, D. G. Rothe, E. M. Hankiewicz, and B. Trauzettel, Phys. Rev. B **85**, 205425 (2012).

[23] P. Szumniak, S. Bednarek, J. Pawlowski, and B. Partoens, Phys. Rev. B **87**, 195307 (2013).

[24] E. Barnes, J. P. Kestner, N. T. T. Nguyen, and S. Das Sarma, Phys. Rev. B **84**, 235309 (2011).

[25] B. Gerardot, R. Barbour, D. Brunner, P. Dalgarno, A. Badolato, N. Stoltz, P. Petroff, J. Houel, and R. Warburton, Appl. Phys. Lett. **99**, 243112 (2011).

[26] B. Alén, F. Bickel, K. Karrai, R. Warburton, and P. M. Petroff, Appl. Phys. Lett. **83**, 2235 (2003).

[27] M. Atatüre, J. Dreiser, A. Badolato, A. Högele, K. Karrai, and A. Imamoglu, Science **312**, 551 (2006).

[28] X. Xu, Y. Wu, B. Sun, Q. Huang, J. Cheng, D. G. Steel, A. S. Bracker, D. Gammon, C. Emary, and L. J. Sham, Phys. Rev. Lett. **99**, 097401 (2007).

[29] Since the optical excitation conditions were different for the Ramsey and spin-echo experiments (in terms of higher laser intensity and a different angle of incidence), this calibration is not exact. The DT signal is also inverted for the Ramsey fringe measurements and has a more asymmetric line shape that can give rise to offsets.

[30] D. Press, T. D. Ladd, B. Zhang, and Y. Yamamoto, Nature (London) **456**, 218 (2008).

[31] S. E. Economou, L. J. Sham, Y. Wu, and D. G. Steel, Phys. Rev. B **74**, 205415 (2006).

[32] C. E. Pryor and M. Flatte, Appl. Phys. Lett. **88**, 233108 (2006).
[33] J. Berezovsky, M. H. Mikkelsen, N. G. Stoltz, L. A. Coldren, and D. D. Awschalom, Science **320**, 348 (2008).
[34] A. Greilich, S. E. Economou, S. Spatzek, D. R. Yakovlev, D. Reuter, A. D. Wieck, T. L. Reinecke, and M. Bayer, Nat. Phys. **5**, 262 (2009).
[35] E. D. Kim, K. Truex, X. Xu, B. Sun, D. G. Steel, A. S. Bracker, D. Gammon, and L. J. Sham, Phys. Rev. Lett. **104**, 167401 (2010).
[36] S. E. Economou, Phys. Rev. B **85**, 241401(R) (2012).
[37] T. D. Ladd, D. Press, K. De Greve, P. L. McMahon, B. Friess, C. Schneider, M. Kamp, S. Höfling, A. Forchel, and Y. Yamamoto, Phys. Rev. Lett. **105**, 107401 (2010).
[38] E. A. Chekhovich, K. Kavokin, J. Puebla, A. B. Krysa, M. Hopkinson, A. Andreev, A. Sanchez, R. Beanland, M. Skolnick, and A. Tartakovskii, Nat. Nanotechnol. **7**, 646 (2012).
[39] L. Rowan, E. L. Hahn, and W. Mims, Phys. Rev. **137**, A61 (1965).
[40] H. Bluhm, S. Foletti, I. Neder, M. Rudner, D. Mahalu, V. Umansky, and A. Yacoby, Nat. Phys. **7**, 109 (2011).
[41] X. J. Wang, S. Chesi, and W. A. Coish Phys. Rev. Lett. **109**, 237601 (2012).
[42] E. Barnes and S. E. Economou, Phys. Rev. Lett. **107**, 047601 (2011).
[43] S. E. Economou and E. Barnes, arXiv:1312.5741.
[44] W. Yang and L. J. Sham, Phys. Rev. B **85**, 235319 (2012).
[45] R. V. Cherbunin, K. Flisinski, I. Y. Gerlovin, I. V. Ignatiev, M. S. Kuznetsova, M. Yu. Petrov, D. R. Yakovlev, D. Reuter, A. D. Wieck, and M. Bayer, Phys. Rev. B **84**, 041304(R) (2011).
[46] A. Greilich, A. Shabaev, D. R. Yakovlev, A. L. Efros, I. A. Yugova, D. Reuter, A. D. Wieck, and M. Bayer, Science **317**, 1896 (2007).
[47] S. G. Carter, A. Shabaev, S. E. Economou, T. A. Kennedy, A. S. Bracker, and T. L. Reinecke, Phys. Rev. Lett. **102**, 167403 (2009).
[48] For some values of τ, there is more than one solution, in which case we conservatively keep the smallest value of $|\Delta|$.